IEEE Access
Multidisciplinary : Rapid Review : Open Access Journal

Received November 30, 2020, accepted December 9, 2020, date of publication December 14, 2020, date of current version December 29, 2020.

Digital Object Identifier 10.1109/ACCESS.2020.3044363

Analysis and Elimination of Unwanted Resonances for Wideband Reflectarray Antenna Design at Sub-Millimeter Waves

EUN-CHEOL CHOI AND SANGWOOK NAM, (Senior Member, IEEE)
School of Electrical and Computer Engineering, Institute of New Media and Communication, Seoul National University, Seoul 08826, South Korea
Corresponding author: Sangwook Nam (snam@snu.ac.kr)

This work was supported in part by the Center for Advanced Meta-Material funded by the Ministry of Science, ICT, and Future Planning as Global Frontier Project under Grant CAMM-2014M3A6B3063708.

ABSTRACT In this study, unwanted additional resonances are analyzed and a method is developed to eliminate them for wideband offset dual reflectarray antenna at sub-millimeter waves. In the terahertz range, the additional resonances can usually be generated within the target bandwidth, depending on the angle of incidence, which cannot be predicted by the normal incidence characteristics of a reflectarray. To evaluate the effects of the additional resonances, the phase error and element patterns of the reflectarray are checked by using the equivalence principle and full-wave simulation. It is found that the additional resonances result in the performance deterioration of the reflectarray antenna due to undesirable phase variation and element pattern changes. Therefore, a sub-wavelength unit-cell is employed to eliminate the additional resonances so that the phase error and element pattern distortion of the reflectarray elements can be avoided in the target bandwidth even for a large angle of incidence. A reflectarray with the sub-wavelength unit-cell is then designed, fabricated, and measured to show the improved gain and bandwidth performances of the reflectarray demonstrating the validity of the proposed analysis.

INDEX TERMS Angle of incidence, dual reflectarray, higher-order resonances, sub-wavelength, surface wave, wideband.

I. INTRODUCTION

Terahertz (THz) technologies in the frequency range from 0.1–10 THz have been undergoing rapid development. There are great potential applications of THz system, such as short range wireless communication, remote sensing, biological detection, and high revolution imaging [1]–[4]. However, there are a lot of practical challenges for the THz components design and manufactures [5]. In the area of antenna, the alternative antenna technologies such as the reflectarray, transmitarray, and metasurface have been developed to avoid the use of complex feeding networks [6]–[8].

A reflectarray antenna technology combines the advantages of a conductor reflector antenna and phased-array antenna. It can produce the desired radiation pattern by the phase compensation of the incident wave through the array elements [9]. Microstrip reflectarray antennas have attracted considerable attention owing to their printed technique, which cannot be implemented using the conductor reflector antennas. The reflectarray technique is employed in various applications such as phase synthesis, contoured beam and multi-beam production, and beam steering by adjusting the reflection phase of the reflectarray elements [10]–[14]. The reflection phase of the microstrip reflectarray elements is derived by varying the size of the conductor elements. Considering that the adjacent array elements are of similar sizes, the reflection phase can be approximately derived by unit-cell simulations in which the array elements are uniform and infinitely arranged. Generally, a unit-cell simulation is implemented with normal incidence, and the reflection phase and amplitude of the unit-cell are determined by the resonance characteristics. However, additional resonance characteristics as well as the original resonances have been observed with respect to the angle of incidence as surface wave and higher-order resonances [15], [16].

In [15], the additional resonances due to surface wave resonance were described. Because surface wave resonances are almost independent of the conductor elements,

The associate editor coordinating the review of this manuscript and approving it for publication was Debdeep Sarkar.

the proposed reflectarray element did not improve the bandwidth performance within the frequency band of the surface wave mode excitation. In [16], additional resonances due to the higher-order resonance of the conductor elements were analyzed. These higher-order resonances deteriorated the gain bandwidth of the reflectarray antenna. Therefore, through the proposed method of arranging the reflectarray elements, the effects of the additional resonances were reduced, and the gain bandwidth of the reflectarray antenna was improved. The two aforementioned studies addressed the additional resonances due to the surface wave and higher-order modes. However, these unwanted resonances were not eliminated, deteriorating the reflectarray antenna performances. To improve the gain and bandwidth performances significantly, the unwanted resonances of the surface wave and higher-order modes should be eliminated within the target bandwidth.

Nevertheless, the solution of unwanted additional resonances have been hardly investigated in reflectarray technique, even though the resonance characteristics of surface wave is well known for periodic structure in a substrate [17]. Generally, in low frequency band, owing to the electrical thin thickness of substrate, the additional resonances can be disregarded because the frequencies of unwanted resonances are far from the target bandwidth. However, when the electrical thickness of the substrate and incident angle increases, the frequency of the surface wave mode excitation decreases resulting in the performance deterioration of the reflectarray within the target bandwidth. Therefore, in high frequency band such as sub-millimeter wave, the additional resonance characteristics should be considered with respect to the angle of incidences.

In this study, we designed an offset Cassegrain antenna structure with a large angle of incidence, and analyzed the additional resonance characteristics of the surface wave and higher-order mode using a circle diagram and the input impedance of the unit-cell. In addition, to evaluate the effects of the additional resonances, the phase error and element patterns of the reflectarray elements are calculated and analyzed based on the equivalence principle and full-wave simulation. To eliminate additional resonances in the target bandwidth, we replaced the $\lambda/2$ array elements with a sub-wavelength array element considering the angle of incidence.

The remainder of this paper is outlined as follows. Section II describes the geometry of the offset dual Cassegrain reflectarray antenna with a large angle of incidence. Section III provides an analysis of the input impedance according to the angle of incidence and evaluation of the phase error and elements pattern of the sub-reflectarray elements. Next, a sub-wavelength unit-cell is presented to eliminate the additional resonances within the target bandwidth. Section IV discusses the fabrication and measurement of the prototype of the offset dual reflectarray antenna. Finally, Section V provides the conclusion and summary of this work. All simulations were performed using the full-wave CST Microwave Studio.

II. OFFSET DUAL REFLECTARRAY ANTENNA DESIGN

In this study, an offset Cassegrain antenna structure is designed to investigate the performance deterioration of the reflectarray elements considering the large angle of incidence in W-band. Fig. 1 shows a schematic of the offset dual reflectarray antenna. Starting with [18], offset dual reflectarray antennas have been developed previously [13], [14], [19], [20]. In the cassegrain structure, the feed antenna and front-end electronics can be located behind the reflector structure in comparison with front-fed antenna. Therefore, the complication of the feed system and ground noise due to spillover sidelobe can be reduced [21], [22]. Moreover, an offset Cassegrain antenna is advantageous over a symmetric Cassegrain antenna in that the position of the feed horn is convenient and the blockage effect of the sub-reflector can be minimized. In addition, the obtained equivalent focal length is greater than the actual physical distance compared to that in a single reflector antenna [20]. The design procedure of the dual Cassegrain reflector antenna was previously described in [23]. The distance between the phase center of the feed horn and sub-reflector is additionally adjusted in this case to improve the antenna performance. The final parameters of the offset Cassegrain antenna are summarized in Table 1. In this structure, the feed horn is used as the pyramidal horn antenna. The aperture dimension and gain performance of the pyramidal feed horn are 7.5 × 7.5 mm and 17.1 dBi at 90 GHz, respectively. The illumination at the edges of the sub-reflectarray is −14.7 dB. The diameter of the main-reflectarray aperture is 45 mm, which is equivalent to 13.5 λ_0 (f_0 = 90GHz); the focal length is 37 mm; and F/D is 0.822. The angle between the phase center of the feed horn and central position of the sub-reflectarray is 46°, and that between the main focal point and central position of the main-reflectarray is 32°. The required phases of the unit cells arranged on the sub-reflectarray and main-reflectarray are given by (1) and (2), respectively [24]:

$$\psi_m = k_0(\overline{F_s M} - \overrightarrow{r_i} \cdot \hat{r}_0) + \psi_0 \tag{1}$$
$$\psi_s = k_0(\overline{F_1 S} - \overline{F_2 S}) + \psi_0 \tag{2}$$

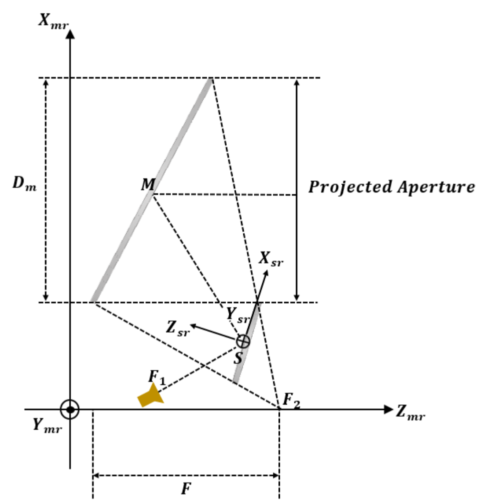

FIGURE 1. Schematic of the offset dual reflectarray antenna.

TABLE 1. Parameters of offset dual reflectarray antenna.

Main-Reflectarray Parameters	
Diameter of the aperture (D_m)	45 mm
Focal distance (F)	37.2
Focus to diameter ratio (F/D)	0.826
Sub-Reflectarray Parameters (data in main-reflectarray coordinate system)	
Center	(13.6, 0, 30.5) mm
Reflectarray size	17.4 x 14 mm
Matrix of direction cosines (Relationship between main- and sub-reflectarray coordinate systems)	$\begin{pmatrix} 0.956 & 0 & 0.293 \\ 0 & -1 & 0 \\ 0.293 & 0 & -0.956 \end{pmatrix}$
Feed Horn (data in sub-reflectarray coordinate system)	
Phase center	(−15.6, 0, 15.3) mm

where k_0 is the free-space wavenumber, $\vec{r}_i$ is the position vector of the i-th element, and $\hat{r}_0$ is the unit vector in the main beam direction. The geometrical parameters of the offset dual reflectaray antenna are as follows: the main focal point (F_2), element positions on the main-reflectarray surface (M), phase center of the feed horn (F_1), and element positions on the sub-reflectarray surface.

III. ADDITIONAL RESONANCE ANALYSIS OF UNIT-CELL

A. λ/2 UNIT-CELL CHARACTERISTICS ALONG THE ANGLE OF INCIDENCE

To obtain the wideband characteristics, the multi-resonance technique of fundamental resonances of unit-cell have been employed as single- and multi-layered structure [25]–[29]. Thus, we used the two layered resonant element as λ/2 unit-cell. Figs. 2 (a) and (b) show the λ/2 unit-cell configuration of two layers consisting of square patches. The dielectric substrates (Duroid 5880) have the following parameters: relative permittivity $\varepsilon_r = 2.2$, loss tangent $\tan\delta = 0.0009$, and a thickness of 0.508 mm. The periodicity of the unit-cell is set at approximately $0.48\lambda_0$ ($f_0 = 90$ GHz), i.e., 1.6 mm, to avoid the generation of a grating lobe. The reflection phase of the λ/2 unit-cell is derived by varying the patch size with a fixed ratio of $p_2 = 0.7p_1$. In general, the reflection phase can be derived using a normal incidence wave because the reflection phase with a moderate incident angle is not significantly different from that with normal incidence. However, when there is a significant change in the angle of incidence, additional resonance characteristics can be observed within the target bandwidth [16]. Therefore, when designing a reflectarray with a large angle of incidence, the resonance characteristics should be investigated according to that angle. For the designed offset cassegrain structure, the incident angles of the sub-reflectarray are approximately 36°–56°. Those are the incident angle of 3dB beam width of the feed horn based on the center position of the sub-reflectarray surface. Thus, we investigated the unit-cell characteristics for a 46° angle of incidence as a representative value. Fig. 3 (a) and (b)

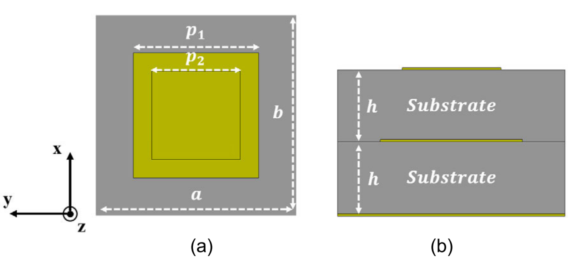

FIGURE 2. λ/2 two-layered unit cell geometry. (a) Top view and (b) side view of the unit cell (corresponding to p_1 = 0.2–1.6mm, $p_2 = 0.7p_1$).

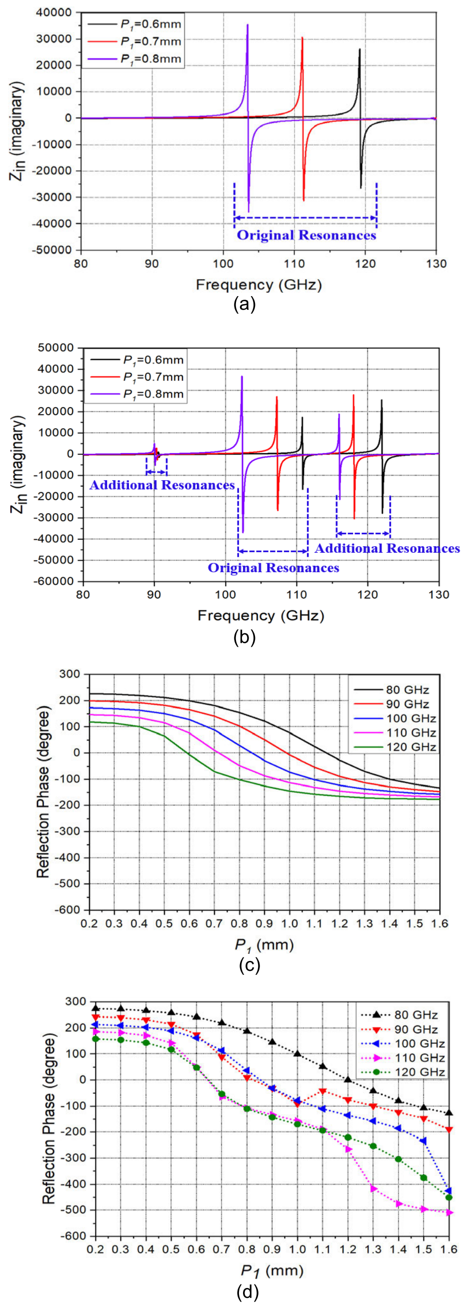

FIGURE 3. Input impedance (imaginary part) and reflection phase of the λ/2 unit cell. (a) Input impedance with normal incidence, (b) input impedance with 46° incidence, (c) reflection phase with normal incidence, and (d) reflection phase with 46° incidence.

represent the input impedance of a $\lambda/2$ unit-cell depending on the angle of incidence at $p_2 = 0.7$–0.9 mm. In the case of normal incidence, the original resonances between 95 and 110 GHz are shown in Figs. 3 (a). However, when the angle of incidence is set to 46°, additional resonances are obtained near the 90- and 118-GHz bands, as shown in Fig. 3 (b). These additional resonances significantly change the unit-cell characteristics. Figs. 3 (c) and (d) represent the reflection phase of the unit-cell according to the angle of incidence. In the case of normal incidence, the reflection-phase range is 360° at the center frequency of 90 GHz and the reflection characteristics show the same trend in all frequency bands. However, in the case of a 46° angle of incidence, the reflection phase shows a significant phase shift from 90–120 GHz owing to the additional resonances. In particular, the reflection phase at 100–120 GHz satisfies the phase range of $\leq 360°$ for normal incidence, but the reflection phase is severely shifted to more than 600° for the 46° angle of incidence.

To investigate the origin of the additional resonances, the resonant frequency is calculated from the surface-wave mode. For $y_{mn}^{TM} = 0$, which is the equivalent admittance of the current source at the air-dielectric interface, a singularity is observed in the Floquet impedance. This singularity is associated with a surface wave mode. Therefore, the blindness of the surface wave of the TM mode can be calculated as follows [17]:

$$y_{mn}^{TM} = Y_{mn}^{TM+} - jY_{mn}^{TM-}\cot(k_{zmn}^{-}h) = 0 \tag{3}$$

where Y_{mn}^{TM} is the modal admittance with $Y_{mn}^{TM+} = k_{zmn}^{+}/\omega\mu_0$ and $Y_{mn}^{TM-} = k_{zmn}^{-}/\omega\mu_0$, for

$$k_{zmn}^{+} = \sqrt{k_0^2 - k_{\rho mn}^2},\ k_{zmn}^{-} = \sqrt{\varepsilon_r k_0^2 - k_{\rho mn}^2} \tag{4}$$

where k_{zmn}^{+} and k_{zmn}^{-} are the wave numbers in the z-direction of air and the dielectric, respectively. The surface wave propagation constant $k_{\rho mn}$ of the TM_0 mode is numerically calculated from (3) and (4). Table 2 shows the calculated $k_{\rho mn}$ of the TM_0 mode according to the different frequencies. In addition, the $k_{\rho mn}$ can be mathematically expressed as

$$\begin{aligned}(k_{\rho mn}/k_0)^2 &= (k_{xmn}/k_0)^2 + (k_{ymn}/k_0)^2 \\ &= \left(\frac{m}{a/\lambda} + u\right)^2 + \left(\frac{n}{b/\lambda} + v\right)^2\end{aligned} \tag{5}$$

TABLE 2. **Calculated surface wave propagation constant $k_{\rho mn}$ of the TM_0 mode.**

Frequency (GHz)	$k_{\rho mn}$	Frequency (GHz)	$k_{\rho mn}$
80	2185	105	3002
85	2348	110	3165
90	2512	115	3328
95	2676	120	3490
100	2839	125	3652

where $u = sin\theta cos\phi$, $v = sin\theta sin\phi$. Fig. 4 shows circle diagrams of the surface wave modes and the (0, 0) Floquet mode, which are represented by the dashed and solid lines, respectively. In the E-plane, the first resonant frequency of the surface wave mode is given by

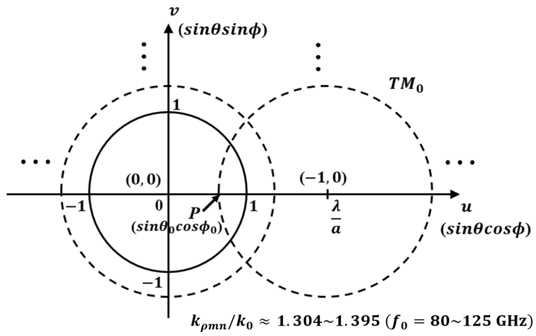

FIGURE 4. **Circle diagram for the surface wave mode and (0, 0) Floquet mode (angle of incidence $\theta_0 = 46°$, $\phi_0 = 0°$).**

$$k_0 \sin\theta_0 \cos\phi_0 + k_{\rho mn} = \frac{2\pi}{a} \tag{6}$$

When the angle of incidence is set to $\theta_0 = 46°, \phi_0 = 0°$, as shown in Fig. 3, the frequency of TM_0 mode surface wave excitation calculated from (6) is 91 GHz. As shown in Fig. 3 (b), the calculated resonant frequency from the surface wave mode is almost identical to the first additional resonances occurring near 90 GHz. Furthermore, the first additional resonances exhibit almost no frequency shift for different element sizes. It is expected that the resonant frequency from the surface wave mode is almost independent of the conductor element pattern. In addition, the second resonant frequency from the surface wave is generated by the $(-1, -1)$ surface wave mode circle and is calculated to be 145 GHz. However, as the second resonant frequency from the surface wave is higher than the target frequency band, it can be disregarded in the design of the proposed structure. As shown in Fig. 4, when the angle of incidence θ_0 is greater, the resonant frequency due to the surface wave mode is lower. Therefore, in structures with large angles of incidence, the resonance characteristics generated from the surface wave mode should always be considered.

In [16], when the angle of incidence was varied, the surface current of the original resonance exhibited the same current distribution as in the normal incidence case. However, the additional resonances from the higher-order mode can occur at other frequency bands in addition to the original resonant-frequency band, and the surface current of the additional resonance exhibits a current distribution different from that of the original resonance. As shown in Fig. 3 (b), the second additional resonances near the 118 GHz band are considered to be due to the higher-order resonance of the unit-cell. This resonance characteristic depends on the dimension of the unit-cell, dielectric constant, and pattern of the conductor elements [30]. Therefore, the second additional resonance near the 118-GHz band exhibits a large frequency shift based on the different element sizes, as compared to the first additional resonance generated by the surface wave mode.

To evaluate the effects of the additional resonances, we analyzed the sub-reflectarray elements because the angle of incidence on the sub-reflectarray is larger than that on the main-reflectarray. The reflectarray elements of the sub-reflector surface is designed with the unit-cell considering a 46° angle of incidence. Fig. 5 presents gain performance of the sub-reflectarray with a feed horn located at focal point. It is equivalent to that of the feed horn located at main focal point F_2 without the sub-reflectarray structure. Therefore, the gain performance of the sub-reflectarray with a feed horn is same as the feed horn itself if the designed reflection phase is obtained in sub-reflectarray. However, as expected, due to the unwanted resonances within the target frequency band, the gain performance deteriorates significantly around 90 and 118 GHz. Therefore, to evaluate the origin of the performance degradation, the reflection phase error and element patterns are calculated based on the equivalence principle and full-wave simulation. The equivalence principle can be employed to calculate the radiation patterns of ideal aperture antennas using the equivalent current sources on the aperture surface [31], [32]. However, to obtain the equivalent current sources of the actual reflectarray elements, we utilized the full-wave simulation results for the proposed reflectarray antenna. Fig. 6 depicts the equivalent current source sampling in the reference plane of the reflectarray elements. The sampling interval is set to 0.02 mm. Thus, in one reflectarray element (λ/2), the equivalent current sources of 6400 points are

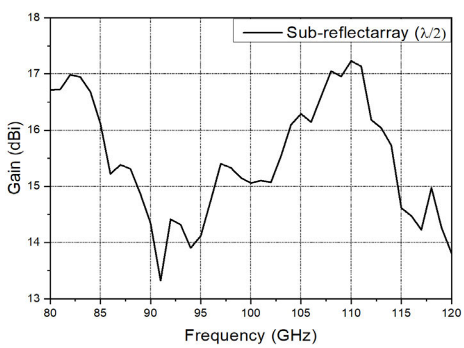

FIGURE 5. Simulated gain performance of the sub-reflectarray composed of the λ/2 reflectarray elements.

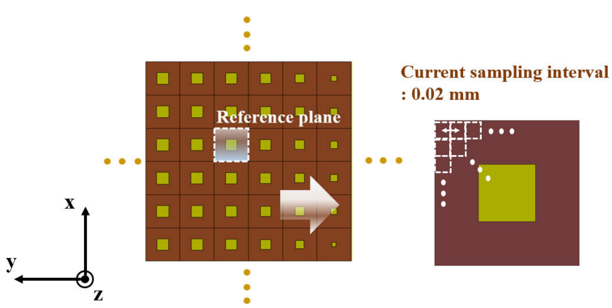

FIGURE 6. Setting the reference plane and current sampling of reflectarray elements for calculating the real element characteristics.

obtained. Moreover, the full-wave simulated reflection phase error and element patterns are calculated using both the equivalent electric and magnetic currents. Fig. 7 presents the real relative phase error and element patterns of sub-reflectarray elements for different frequencies based on the equivalent principle and full-wave simulation. The real relative phase error of the reflectarray elements is defined by the reflection phase error of the actual reflectarray elements with respect to that of the central element [16]. As shown in Figs. 7 (a) – (c), the relative phase errors of edge elements are significant although the reflectarray elements of the sub-reflector is designed with the unit-cell considering a 46° angle of incidence. Figs. 7 (d)–(f) show the element patterns arranged on the half plane of the sub-reflectarray surface. The element patterns for 80 GHz are not distorted, but those corresponding to 90 and 120 GHz are significantly distorted. These pattern distortions at 90 and 120 GHz are caused by the surface wave loss and current distribution change due to the higher-order mode, respectively. In addition, the reflected angle of the sub-reflectarray is approximately 40°. Notice that in around reflected angle 40°, more elements exhibit lower intensities (<-10 dB) at 90 and 120 GHz compared with 80 GHz. Thus, it is concluded that the gain deterioration of the sub-reflectarray is caused by the element pattern distortion and reflection phase error due to the effects of the unwanted resonances. Fig. 8 shows the simulated gain performance of the dual reflectarray antenna consisting of λ/2 unit-cells at different frequencies. The gain performance shows the maximum gain of 28.5 dBi at 84 GHz and maximum efficiency of 43.5% at 79 GHz. The gain and efficiency of 25.8 dBi and 21.1%, respectively, represent low performance at the center frequency of 90 GHz. In addition, a narrow 1-dB gain bandwidth of 8 GHz (8.8%) is obtained from 78 to 85 GHz. Therefore, it is expected that low performance of the dual reflectarray antenna with λ/2 unit cells is caused by the effects of the unwanted resonances due to the large angle of incidence.

B. SUB-WAVELENGTH UNIT-CELL CHARACTERISTICS ALONG THE ANGLE OF INCIDENCE

As described in Section III.-A, the additional resonance characteristics based on the angle of incidence can cause element pattern distortion and reflection phase error, resulting in antenna performance degradation. Therefore, to achieve the desired performance, the additional resonance characteristics within the target bandwidth should be eliminated. In the case of resonance from the surface wave mode, the intersection between the (0, 0) Floquet-mode and surface wave mode circles in Fig. 4 induces surface-wave resonance characteristics. Therefore, to eliminate the additional resonances within the target frequency band, we used a sub-wavelength unit-cell with small periodicity. So far, sub-wavelength unit-cells have been employed for wideband characteristics [33]–[38]. However, the relationship between sub-wavelength unit-cell with small periodicity and the additional resonances has not been sufficiently described.

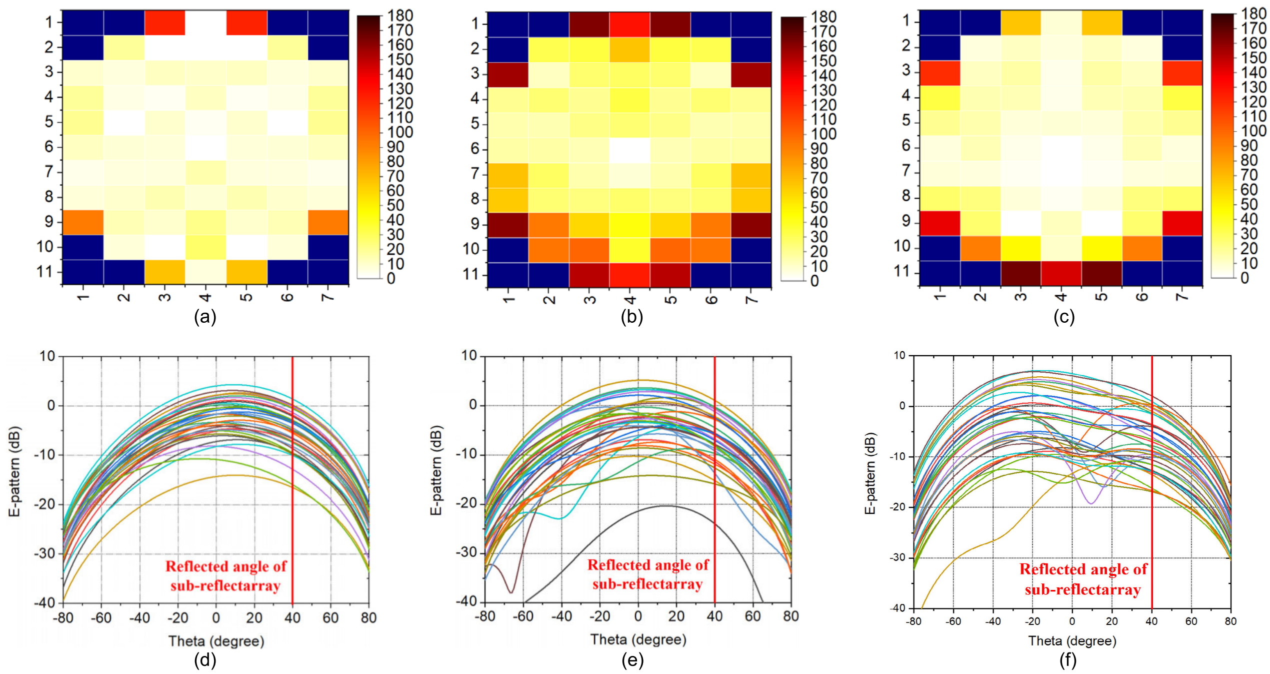

FIGURE 7. Real relative phase errors and element patterns of the sub-reflectarray composed of $\lambda/2$ elements based on the equivalence principle and full-wave simulation. (a) Relative phase error at 80 GHz (original resonance), (b) 90 GHz (surface wave resonance), (c) 120 GHz (higher-order resonance), and (d) element patterns at 80 GHz (original resonance), (e) 90 GHz (surface wave resonance), (f) 120 GHz (higher-order resonance).

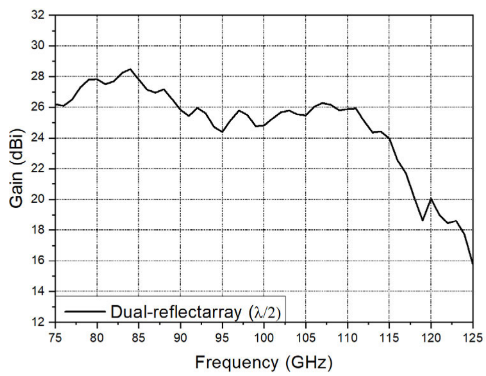

FIGURE 8. Simulated gain characteristics of dual reflectarray composed of $\lambda/2$ elements.

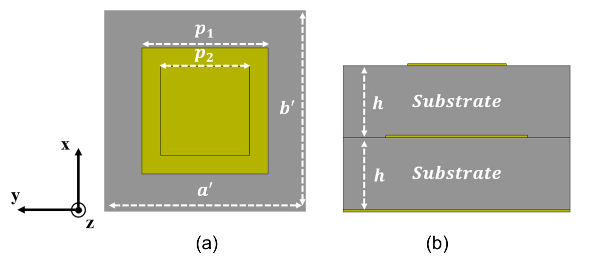

FIGURE 9. Proposed sub-wavelength unit-cell structure. (a) Top view and (b) side view of unit cell.

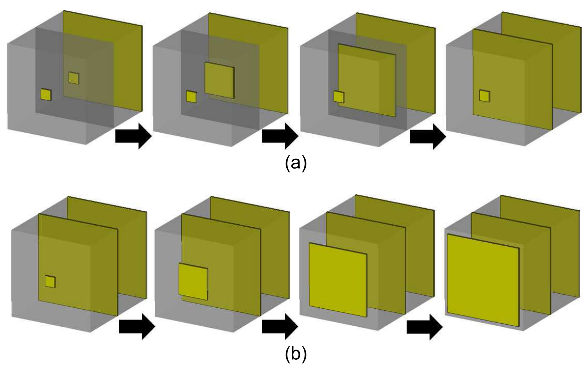

FIGURE 10. Proposed dimension variation of sub-wavelength unit-cell according to different steps. (a) Step 1 and (b) step2.

Fig. 9 shows the proposed sub-wavelength unit-cell geometry. As in the $\lambda/2$ unit-cell case, a double-layer substrate of Duroid 5880 is used and the periodicity is periodicity is reduced. Table 3 summarizes the variation method of the proposed unit-cell. To reduce the phase sensitivity, the elements of the proposed unit-cell are varied individually, unlike in the conventional variation method of changing the elements simultaneously. Fig. 10 shows the proposed variation method according to different steps. The dimension variation of the sub-wavelength unit-cell is as follow: p_1 is varied between 0.1 to a' mm where p_2 is fixed to 0.1mm, and then p_2 is varied between 0.1 to ($a' - 0.03$) mm where p_1 is fixed to a' mm.

To determine the periodicity of the sub-wavelength unit-cell, the characteristics of the sub-wavelength unit-cell are simulated with respect to the different periodicities. Fig. 11 shows the reflection phase of sub-wavelength unit-cells. Table 4 shows the total phase range and calculated resonant frequency of the surface wave mode of the

TABLE 3. Geometric parameters of the proposed variation method.

Parameters (mm)	p_1	p_2	h
Step 1	0.1 to a′	0.1	0.508
Step 2	a′	0.1 to (a′ − 0.03)	0.508

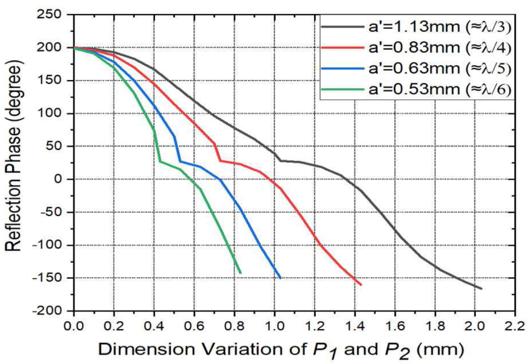

FIGURE 11. Reflection phase of the unit-cell according to the angle of incidence at f_0 = 90GHz.

TABLE 4. Total phase range and frequency of TM_0 mode surface wave excitation.

Periodicity (a′)	Total phase range	Resonant frequency of surface wave at θ_0=46°, ϕ_0=0°.
1.13 mm (≈ λ/3)	371°	127 GHz
0.83 mm (≈ λ/4)	360°	168 GHz
0.63 mm (≈ λ/5)	338°	219 GHz
0.53 mm (≈ λ/6)	331°	262 GHz

sub-wavelength unit-cell from (3)–(6). As the periodicity of the unit-cell is reduced, the total reflection phase range of unit-cell is reduced and the resonant frequency of the surface wave mode increases. To obtain the high efficiency performance of reflectarray antenna, at least 360° phase range of the unit-cell should be obtained and the additional resonances of the surface wave mode should be eliminated within the target bandwidth. Thus, considering the characteristics of the sub-wavelength unit-cell, the periodicity of the sub-wavelength unit-cell to 0.83mm (λ/4) is selected. In the proposed sub-wavelength (λ/4) unit-cell, the resonant frequency from the (−1, 0) surface wave mode is calculated to be 168 GHz. This resonance frequency of the surface wave mode can be disregarded because it is not in the target bandwidth. Figs. 12 (a) and (b) show the imaginary part of the input impedance of a sub-wavelength (λ/4) unit-cell depending on the angle of incidence at $p_1 = 0.5$–0.8 mm. Unlike the λ/2 unit-cell, the sub-wavelength unit-cell shows a frequency shift due to the variation in wave number according to the angle of incidence. Thus, no additional resonance characteristic is generated in the desired frequency band. In addition, owing to the different conductor element variation method and reduced periodicity of the unit-cell, the additional resonances from the higher-order resonance of the unit-cell are further shifted to a higher frequency band. Figs. 12 (c) and (d)

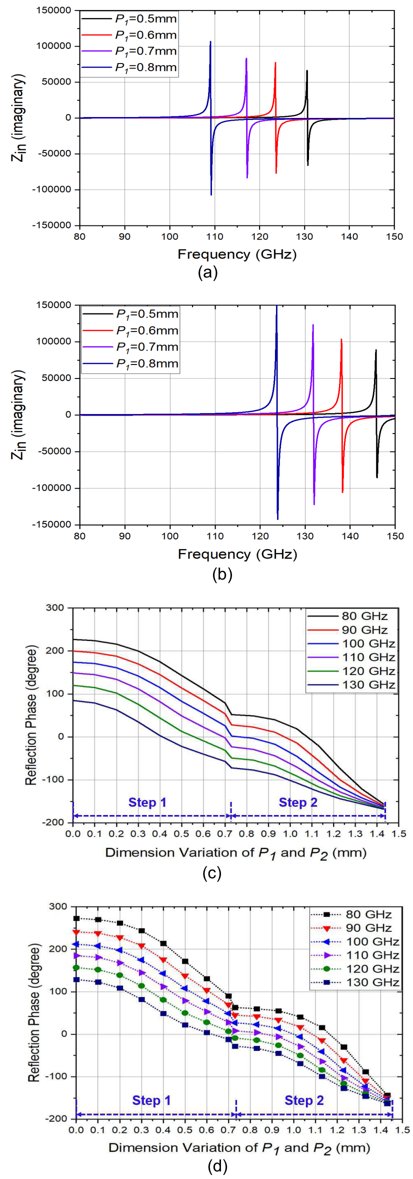

FIGURE 12. Input impedance (imaginary part) and reflection phase of the λ/4 unit cell. (a) Input impedance with normal incidence, (b) input impedance with 46° incidence, (c) reflection phase with normal incidence, and (d) reflection phase with 46° incidence.

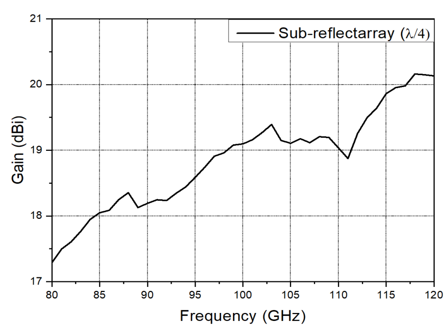

FIGURE 13. Gain performance of the sub-reflectarray composed of the sub-wavelength (λ/4) reflectarray elements.

show the reflection phase of the sub-wavelength unit-cell based on the angle of incidence. As the additional resonances are eliminated in the target frequency band,

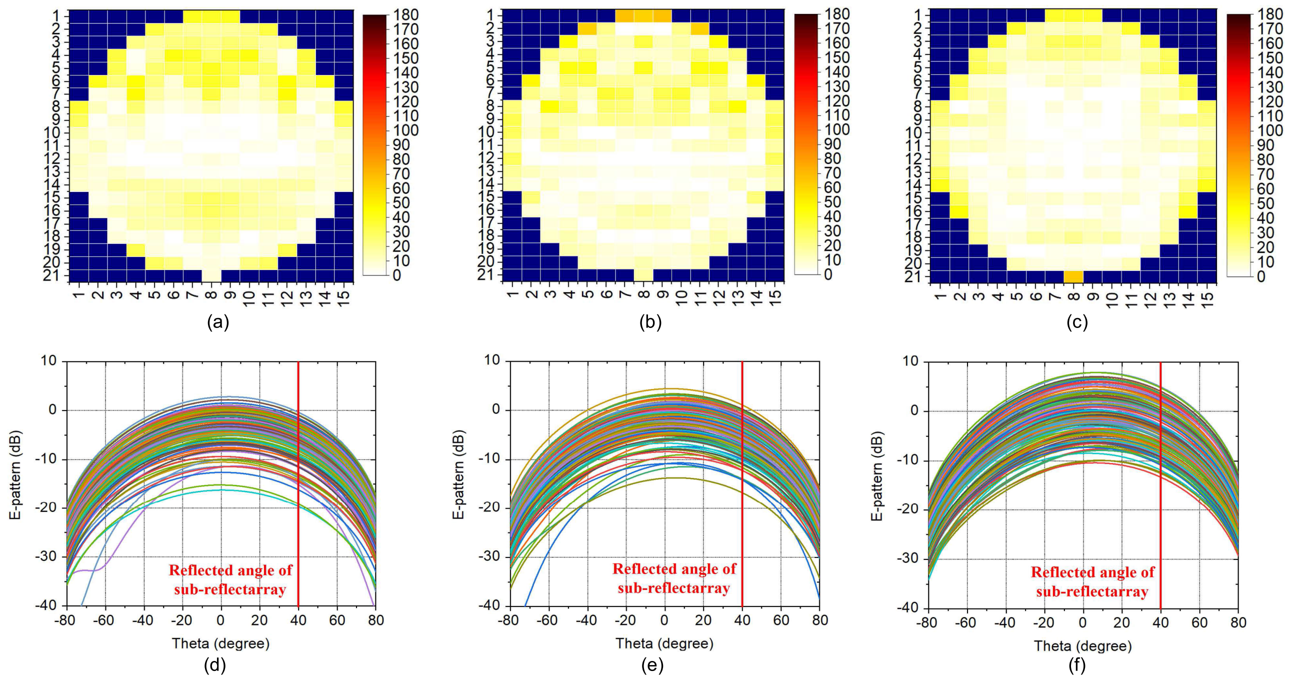

FIGURE 14. Real relative phase errors and element patterns of the sub-reflectarray composed of the sub-wavelength ($\lambda/4$) elements based on the equivalence principle and full-wave simulation. (a) Relative phase error at 80 GHz, (b) 90 GHz, (c) 120 GHz, and (d) element patterns at 80 GHz, (e) 90 GHz, (f) 120 GHz.

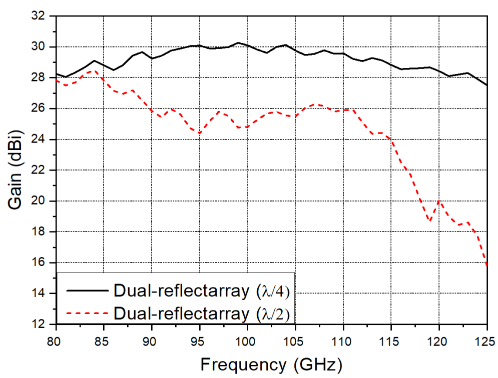

FIGURE 15. Simulated gain characteristics of dual reflectarray composed of the sub-wavelength ($\lambda/4$) and $\lambda/2$ elements.

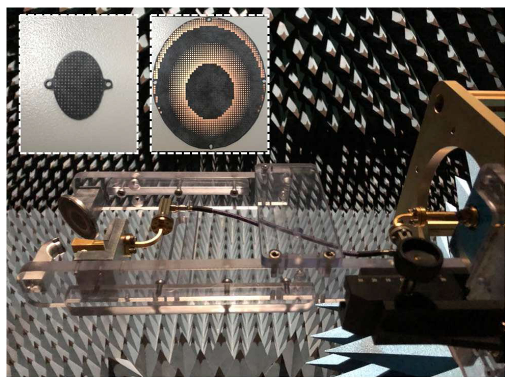

FIGURE 16. Fabricated prototype of proposed reflectarray antenna composed of the sub-wavelength ($\lambda/4$) elements.

the reflection phase is not significantly shifted. The reflection phase range for normal and oblique incidence at the center frequency of 90 GHz is approximately 360° and 400°, respectively. Fig. 13 shows the simulated gain performance of the sub-reflectarray designed with the sub- wavelength unit-cell. The gain performances are not deteriorated within the target frequency band due to the elimination of the additional resonances. Fig. 14 represents the real relative phase error and element patterns of array elements of the sub-reflectarray designed with the sub-wavelength unit-cell based on the equivalence principle and full-wave simulation. Compared with the sub-reflectarray with the $\lambda/2$ unit-cell, the relative phase errors are generally very low across the entire sub-reflector surface. In addition, the element patterns are not distorted within the target frequency band. These results are correlated with the gain performance of the sub-reflectarray designed with the sub- wavelength unit-cell. Fig. 15 shows the simulated gain performance of the offset dual reflectarray consisting of sub- wavelength unit-cells at different frequencies. The simulated gain performance shows a maximum gain of 30.1 dBi at 104 GHz and a maximum efficiency of 52.6 % at 89 GHz. At the center frequency of 90 GHz, a peak gain of 29.2 dBi and an efficiency of 46.7 % are obtained. The 1-dB gain bandwidth of 26 GHz (28.8%) from 88 to 114 GHz and the 2-dB gain bandwidth of 45 GHz (50%) from 78 to 123 GHz are widely satisfied.

Due to the elimination of the unwanted surface wave and higher-order resonances, the gain bandwidth and

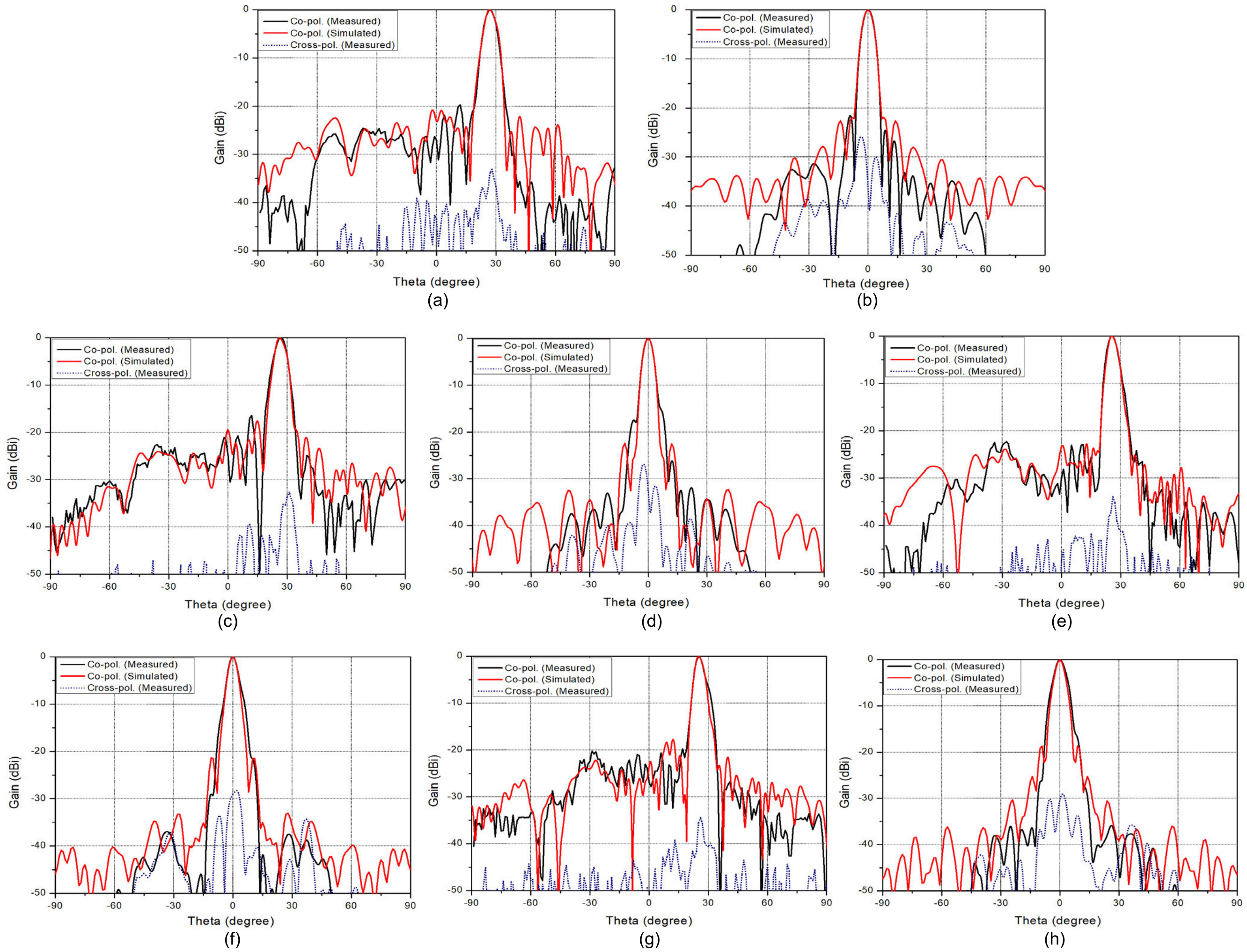

FIGURE 17. Simulated and measured radiation patterns of proposed reflectarray antenna composed of the sub-wavelength ($\lambda/4$) elements on the (a) E-plane and (b) H-plane at 80 GHz; (c) E-plane and (d) H-plane at 90 GHz; (e) E-plane and (f) H-plane at 100 GHz; and (g) E-plane and (h) H-plane at 110 GHz.

efficiency of the proposed sub-wavelength reflectarray antenna are improved compared with those of the reflectarray antenna consisting of $\lambda/2$ unit cells. Thus, when designing a reflectarray structure with a large angle of incidence, a sub-wavelength unit cell is considered to be a good candidate for the reflectarray elements.

IV. EXPERIMENTAL RESULTS

In this study, a W-band dual reflectarray antenna composed of the sub-wavelength elements is designed and fabricated, as shown in Fig. 16. The measurements are performed in a millimeter-wave non-directional chamber. To connect the source to the offset feed horn, a 90° waveguide and a transition adapter of a radiofrequency cable are used. For the precise set up of the measurement equipment, the strut of the feed horn is fabricated to adjust the antenna position. The proposed antenna achieves the necessary gain bandwidth within the W-band (75–110 GHz) and D-band (110–170 GHz). However, the measurements is only

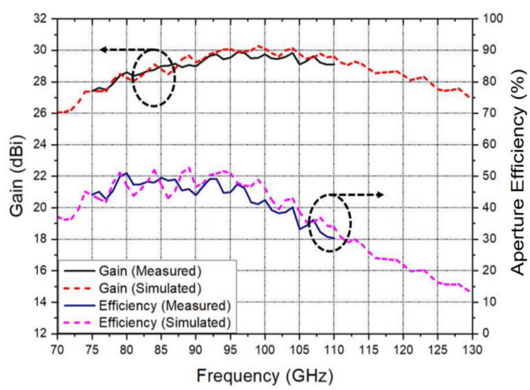

FIGURE 18. Simulated and measured gain and corresponding aperture efficiency of proposed reflectarray antenna composed of the sub-wavelength ($\lambda/4$) elements.

conducted up to the W-band because the measurement module of the radiation pattern in the D-band is not prepared at an authorized radiation-measurement institute. The proposed antenna is designed to have a center frequency of 90 GHz. The simulated and measured radiation patterns in the two principal planes, i.e., the E-and H- planes, are presented in Fig. 17 at 80, 90, 100, and 110 GHz for comparison and to illustrate the wideband antenna performance in the W-band. The radiation pattern of the E-plane is acquired through far-field measurement. The radiation pattern of the H-plane is obtained by performing planar near-field measurements owing to the tilted scan angle. In the measured radiation pattern of the H-plane, some asymmetrical characteristics are observable because a scattering field is detected in the measurement equipment within the planar near-field measurement range. The time required for near-field measurement is significantly longer than that for far-field measurement, limiting the measurement scan range to $\pm 30°$. The side-lobe levels of the E- and H-planes at the center frequency of 90 GHz are -17 and -18 dB, respectively, and the corresponding cross-polarization levels are -33 and -27 dB. The maximum side-lobe and cross-polarization level within the target band are -17 and -26 dB, respectively. Fig. 18 shows the proposed antenna gain and aperture efficiency as functions of frequencies. The maximum aperture efficiency is 51% at 80 GHz. The simulated 1-dB gain bandwidth is approximately 28.8% at 88–114 GHz, and the simulated 2-dB gain bandwidth is 50% at 78–123 GHz. Owing to the deficiency of measurement module above the W-band, the measured 1- and 2-dB gain bandwidths are 28.8% and 35.5%, respectively. However, because the simulated and measured gain performances exhibit similar trend, similar result can be obtained for the simulated and measured gain above the W-band. Table 5 compares the obtained results of previous offset dual reflectarray and single reflectarray antennas with sub-wavelength unit-cell. The proposed reflectarray antenna shows improved bandwidth performance compared with previous offset dual reflectarray antennas. However, due to the structural configuration of offset dual reflectarray with large incident angle, some single reflectarray antennas with sub-wavelength unit-cell and small incident angle show improved performances compared with proposed dual reflectarray.

TABLE 5. Comparison with previous studies of offset dual reflectarray antennas and sub-wavelength unit-cell.

	This Work	[18]3)	[20]3)	[19]3)#	[34]4)	[35]4)	[38]4)
Freq. (GHz)	90	14	8.4 / 31.8	94	10	10	10
Size (λ_0)	13.5	21	21 / 80	37	9.6	9	6.9
Max. Gain (dBi)	29.9	34.5	44.7	38.7	28.2	25.8	25
Periodicity (λ_0)	0.25	0.37	0.5	0.3	0.2	0.33	0.3
F/D	0.82	4	0.64	0.67	1	1	0.71
Max. Effi. (%)	51	65	49.8 / 48.2	53	56.5	39	58.3
1-dB BW. (%)	28.8 1) 28.8 2)	N.A.	N.A.	3	N.A.	17	30
2-dB BW. (%)	35.5 1) 50 2)	N.A.	N.A.	N.A.	N.A.	N.A.	N.A.
2.5-dB BW. (%)	56 2)	20	N.A.	N.A.	N.A.	N.A.	N.A.
3-dB BW. (%)	58.3 2)	N.A	7.1 / 6.3	N.A.	32	N.A.	N.A.

1): Measured Performance,
2): Expected Performance (Confirmed up to 75 to 110 GHz),
3): Offset dual reflectarray structure
4): Single reflectarray structure with subwavelength unit-cell
#: Main reflector is conductor reflector.

V. CONCLUSION

In this study, considering a large angle of incidence, the additional resonances are found to deteriorate the performance of a reflectarray antenna due to the reflection phase error and element pattern distortion at sub-millimeter wave. The analysis confirmed that the additional resonances are due to the surface waves and higher-order modes. The effects of the additional resonances are evaluated by calculating the phase error and the element patterns of the reflectarray elements based on the equivalence principle and full-wave simulation. It is found that, to eliminate the additional resonances within the target bandwidth, sub-wavelength unit-cells can be used as the reflectarray elements. This approach improves the phase error and element pattern distortion of the reflectarray elements as well as the gain and bandwidth of the proposed reflectarray antenna. Further, a W-band offset dual reflectarray antenna with wideband characteristics is designed and fabricated, and its performance is verified. The measured gain is 28.9 dBi at 90 GHz and the maximum efficiency is 51% at 80 GHz. The simulated 1- and 2-dB gain bandwidths are approximately 28.8% and 50%, respectively. Owing to the deficiency of the measurement module, the measured 1- and 2-dB gain bandwidths are approximately 28.8% and 35.5%, respectively.

REFERENCES

[1] J. F. Federici, "THz imaging and sensing for security applications-explosives, weapons and drugs," *Semicond. Sci. Technol.*, vol. 20, no. 7, pp. 266–280, 2005.

[2] P. H. Siegel, "Terahertz technology," *IEEE Trans. Microw. Theory Techn.*, vol. 50, no. 3, pp. 910–928, Mar. 2002.

[3] E. R. Mueller, "Terahertz radiation: Applications and sources," *Ind. Phys.*, vol. 9, no. 4, pp. 27–30, 2003.

[4] H.-J. Song and T. Nagatsuma, "Present and future of terahertz communications," *IEEE Trans. THz Sci. Technol.*, vol. 1, no. 1, pp. 256–263, Sep. 2011.

[5] P. H. Siegel, P. de Maagt, and A. I. Zaghloul, "Antennas for terahertz applications," in *Proc. IEEE Antennas Propag. Soc. Int. Symp.*, May 2006, pp. 2383–2386.

[6] D. M. Pozar, S. D. Targonski, and H. D. Syrigos, "Design of millimeter wave microstrip reflectarrays," *IEEE Trans. Antennas Propag.*, vol. 45, no. 2, pp. 287–296, 1997.

[7] C. G. M. Ryan, M. R. Chaharmir, J. Shaker, J. R. Bray, Y. M. M. Antar, and A. Ittipiboon, "A wideband transmitarray using dual-resonant double square rings," *IEEE Trans. Antennas Propag.*, vol. 58, no. 5, pp. 1486–1493, May 2010.

[8] Q. Yang, J. Gu, D. Wang, X. Zhang, Z. Tian, C. Ouyang, R. Singh, J. Han, and W. Zhang, "Efficient flat metasurface lens for terahertz imaging," *Opt. Exp.*, vol. 22, no. 21, pp. 25931–25939, Oct. 2014.

[9] J. Huang and J. A. Encinar, *Reflectarray Antennas*. Piscataway, NJ, USA: IEEE Press, 2007.

[10] Leberer, Ralf, and Wolfgang Menzel, "A dual planar reflectarray with synthesized phase and amplitude distribution," *IEEE Trans. Antennas Propag.*, vol. 53, no. 11, pp. 3534–3539, 2005.

[11] J. A. Encinar and J. A. Zornoza, "Three-layer printed reflectarrays for contoured beam space applications," *IEEE Trans. Antennas Propag.*, vol. 52, no. 5, pp. 1138–1148, May 2004.
[12] P. Nayeri, F. Yang, and A. Z. Elsherbeni, "Design and experiment of a single-feed quad-beam reflectarray antenna," *IEEE Trans. Antennas Propag.*, vol. 60, no. 2, pp. 1166–1171, Feb. 2012.
[13] E. Martinez-de-Rioja, J. A. Encinar, R. Florencio, and C. Tienda, "3-D bifocal design method for dual-reflectarray configurations with application to multibeam satellite antennas in ka-band," *IEEE Trans. Antennas Propag.*, vol. 67, no. 1, pp. 450–460, Jan. 2019.
[14] E. Martinez-de-Rioja, J. A. Encinar, A. G. Pino, B. Gonzalez-Valdes, S. V. Hum, and C. Tienda Herrero, "Bifocal design procedure for dual-reflectarray antennas in offset configurations," *IEEE Antennas Wireless Propag. Lett.*, vol. 17, no. 8, pp. 1421–1425, Aug. 2018.
[15] J. H. Yoon and Y. J. Yoon, "Bandwidth enhancement of single-layer microstrip reflectarrays with multi-dipole elements," *J. Electromagn. Eng. Sci.*, vol. 19, no. 2, pp. 130–139, Apr. 2019.
[16] E.-C. Choi and S. Nam, "W-band low phase sensitivity reflectarray antennas with wideband characteristics considering the effect of angle of incidence," *IEEE Access*, vol. 8, pp. 111064–111073, 2020.
[17] A. K. Bhattacharyya, *Phased Array Antennas: Floquet Analysis, Synthesis, BFNs and Active Array Systems*. vol. 179. Hoboken, NJ, USA: Wiley, 2006.
[18] C. Tienda, J. A. Encinar, M. Arrebola, M. Barba, and E. Carrasco, "Design, manufacturing and test of a dual-reflectarray antenna with improved bandwidth and reduced cross-polarization," *IEEE Trans. Antennas Propag.*, vol. 61, no. 3, pp. 1180–1190, Mar. 2013.
[19] W. Hu, M. Arrebola, R. Cahill, J. A. Encinar, V. Fusco, H. S. Gamble, Y. Alvarez, and F. Las-Heras, "94 GHz dual-reflector antenna with reflectarray subreflector," *IEEE Trans. Antennas Propag.*, vol. 57, no. 10, pp. 3043–3050, Oct. 2009.
[20] C. Han, J. Huang, and K. Chang, "Cassegrain offset subreflector-fed X/Ka dual-band reflectarray with thin membranes," *IEEE Trans. Antennas Propag.*, vol. 54, no. 10, pp. 2838–2844, Oct. 2006.
[21] R. Chatterjee, *Antenna Theory and Practice*. New Delhi, India: New Age International, 1996.
[22] W. J. Welch, "1.2. types of astronomical antennas," in *Methods in Experimental Physics*, vol. 12. New York, NY, USA: Academic, 1976, pp. 7–28.
[23] C. Granet, "Designing classical offset cassegrain or gregorian dual-reflector antennas from combinations of prescribed geometric parameters," *IEEE Antennas Propag. Mag.*, vol. 44, no. 3, pp. 114–123, Jun. 2002.
[24] E. Almajali, D. McNamara, J. Shaker, and M. R. Chaharmir, "Derivation and validation of the basic design equations for symmetric sub-reflectarrays," *IEEE Trans. Antennas Propag.*, vol. 60, no. 5, pp. 2336–2346, May 2012.
[25] J. A. Encinar, "Design of two-layer printed reflectarrays using patches of variable size," *IEEE Trans. Antennas Propag.*, vol. 49, no. 10, pp. 1403–1410, 2001.
[26] M. Bozzi, S. Germani, and L. Perregrini, "Performance comparison of different element shapes used in printed reflectarrays," *IEEE Antennas Wireless Propag. Lett.*, vol. 2, pp. 219–222, 2003.
[27] P. Nayeri, F. Yang, and A. Z. Elsherbeni, "Broadband reflectarray antennas using double-layer subwavelength patch elements," *IEEE Antennas Wireless Propag. Lett.*, vol. 9, pp. 1139–1142, 2010.
[28] M. Mohammadirad, N. Komjani, M. R. Chaharmir, J. Shaker, and A. R. Sebak, "Impact of feed position on the operating band of broadband reflectarray antenna," *IEEE Antennas Wireless Propag. Lett.*, vol. 11, pp. 1104–1107, 2012.
[29] X. Xia, Q. Wu, H. Wang, C. Yu, and W. Hong, "Wideband millimeter-wave microstrip reflectarray using dual-resonance unit cells," *IEEE Antennas Wireless Propag. Lett.*, vol. 16, pp. 4–7, 2017.
[30] Kristensson, Gerhard, "On the generation of surface waves in frequency selective structures," Dept. Electrosci. Electromagn. Theory, Lund Inst. Technol. Sweden, Lund, Sweden, 2003.
[31] C. A. Balanis, *Antenna Theory: Analysis and Design*. Hoboken, NJ, USA: Wiley, 2016.
[32] Nayeri, Payam, Fan Yang, and Atef Z. Elsherbeni. *Reflectarray Antennas: Theory, Designs and Applications*. Hoboken, NJ, USA: Wiley, 2018.
[33] E. R. F. Almajali and D. A. McNamara, "Angle of incidence effects in reflectarray antenna design: Making gain increases possible by including incidence angle effects.," *IEEE Antennas Propag. Mag.*, vol. 58, no. 5, pp. 52–64, Oct. 2016.
[34] P.-Y. Qin, Y. J. Guo, and A. R. Weily, "Broadband reflectarray antenna using subwavelength elements based on double square meander-line rings," *IEEE Trans. Antennas Propag.*, vol. 64, no. 1, pp. 378–383, Jan. 2016.
[35] G. Zhao, Y.-C. Jiao, F. Zhang, and F.-S. Zhang, "A subwavelength element for broadband circularly polarized reflectarrays," *IEEE Antennas Wireless Propag. Lett.*, vol. 9, pp. 330–333, 2010.
[36] L. Guo, P.-K. Tan, and T.-H. Chio, "Single-layered broadband dual-band reflectarray with linear orthogonal polarizations," *IEEE Trans. Antennas Propag.*, vol. 64, no. 9, pp. 4064–4068, Sep. 2016.
[37] C. Han, Y. Zhang, and Q. Yang, "A broadband reflectarray antenna using triple gapped rings with attached phase-delay lines," *IEEE Trans. Antennas Propag.*, vol. 65, no. 5, pp. 2713–2717, May 2017.
[38] H. Yu and L. Guo, "Broadband single-layer reflectarray antenna employing circular ring elements dented with sectorial slits," *IEEE Access*, vol. 7, pp. 165814–165819, 2019.

EUN-CHEOL CHOI received the B.S. and M.S. degrees in electronics, telecommunications and computer engineering from Korea Aerospace University, Goyang, South Korea, in 2012 and 2014, respectively, and the Ph.D. degree from Seoul National University, Seoul, South Korea, in 2020.

He is currently working as a Postdoctoral Researcher with Seoul National University. His research interests include micro-wave and millimeter-wave, and reflectarray antenna design and analysis.

SANGWOOK NAM (Senior Member, IEEE) received the B.S. degree from Seoul National University, Seoul, South Korea, in 1981, the M.S. degree from the Korea Advanced Institute of Science and Technology (KAIST), Seoul, in 1983, and the Ph.D. degree from The University of Texas at Austin, Austin, TX, USA, in 1989, all in electrical engineering. From 1983 to 1986, he was a Researcher with the Gold Star Central Research Laboratory, Seoul. Since 1990, he has been a Professor with the School of Electrical Engineering and Computer Science, Seoul National University. His research interests include analysis/design of electromagnetic (EM) structures, antennas, and microwave active/passive circuits.